

TOPICAL REVIEW

Effects of 3D Magnetic Perturbations on Toroidal Plasmas

J.D. Callen

University of Wisconsin, Madison, WI 53706-1609 USA

E-mail: callen@engr.wisc.edu, <http://homepages.cae.wisc.edu/~callen>

Abstract. Small three-dimensional (3D) magnetic field perturbations have many interesting and possibly useful effects on tokamak and quasi-symmetric stellarator plasmas. Plasma transport equations that include these effects, most notably on diamagnetic-level toroidal plasma flows, have recently been developed. The 3D field perturbations and their plasma effects can be classified according to their toroidal mode number n : low n (say 1 to 5) resonant (with field line pitch, $q = m/n$) and non-resonant fields, medium n (~ 20 , due to toroidal field ripple), and high n (due to microturbulence). Low n non-resonant fields induce a neoclassical toroidal viscosity (NTV) that damps toroidal rotation throughout the plasma toward an offset rotation in the counter-current direction. Recent tokamak experiments have generally confirmed and exploited these predictions by applying external low n non-resonant magnetic perturbations. Medium n toroidal field ripple produces similar effects plus possible ripple trapping NTV effects and ion direct losses in the edge. A low n (e.g., $n = 1$) resonant field is mostly shielded by the toroidally rotating plasma at and inside the resonant (rational) surface. If it is large enough it can stop plasma rotation at the rational surface, facilitate magnetic reconnection there and lead to a growing stationary magnetic island (locked mode), which often causes a plasma disruption. Externally applied 3D magnetic perturbations usually have many components. In the plasma their lowest n (e.g., $n = 1$) externally resonant components can be amplified by kink-type plasma responses, particularly at high β . Low n plasma instabilities [e.g., resistive wall modes (RWMs), neoclassical tearing modes (NTMs)] cause additional 3D magnetic perturbations in tokamak plasmas. Tearing modes in their nonlinear (Rutherford) regime bifurcate the topology and form magnetic islands. Finally, multiple resonant magnetic perturbations (RMPs) can, if not shielded by plasma rotation effects, cause local magnetic stochasticity and increase plasma transport in the edge of H-mode plasmas. These various effects of 3D fields can be used to modify directly the plasma toroidal rotation [and possibly transport via multiple RMPs for controlling edge localized modes (ELMs)] and indirectly anomalous plasma transport. The present understanding and modeling of these various 3D magnetic field perturbation effects including for test blanket modules (TBMs) in ITER are summarized. Finally, implications of the present understanding and key open issues for developing a predictive capability of them for ITER are discussed.

PACS numbers: 52.55.Dy, 52.55.Fa, 52.30.Ex, 52.55.Hc, 52.25.Xz

1. Introduction, Magnetic Field

Background: Recently there has been increasing interest in and research on the effects of small three-dimensional (3D) magnetic field perturbation effects on tokamak plasmas. Also, possible effects and uses of 3D fields in ITER [1, 2] are being explored. This theory-based overview paper summarizes the present status of such studies.

Magnetic field representation: Tokamaks are two-dimensional (2D) axisymmetric magnetic systems to lowest order with a magnetic field \mathbf{B}_0 . But small 3D perturbations $\delta\mathbf{B}$ arise from externally applied fields (field errors, control coils and toroidal field ripple) and plasma instabilities. Using the poloidal magnetic flux ψ (radial coordinate), straight-field-line poloidal angle θ and axisymmetric toroidal angle ζ , the total magnetic field will be represented by $\mathbf{B} = \mathbf{B}_0(\psi, \theta) + \delta\mathbf{B}(\psi, \theta, \zeta)$ with $\mathbf{B}_0 \equiv I\nabla\zeta + \nabla\zeta \times \nabla\psi = \nabla\psi \times \nabla[q(\psi)\theta - \zeta] = \mathbf{B}_t + \mathbf{B}_p$. The magnitude of the \mathbf{B} field in near-axisymmetric tokamaks can be written as

$$|\mathbf{B}| = \underbrace{|\mathbf{B}_0(\psi, \theta)|}_{\text{2D axisymm.}} + \underbrace{\sum_{n,m} \delta B_n(\psi, m) \cos(m\theta - n\zeta - \varphi_{m,n})}_{\text{low } m, n \text{ resonant, non-resonant}} + \underbrace{\delta B_N(\psi, \theta) \cos(N\zeta)}_{\text{medium } n, \text{ ripple}} + \underbrace{\dots}_{\mu\text{turb}}. \quad (1)$$

The 3D magnetic perturbations and their effects on toroidal plasmas can be classified approximately by their toroidal mode number n : low n (1 to 5 or more) resonant (with the magnetic field line pitch, $q=m/n$) and non-resonant fields, medium n (mainly due to ripple from $N \sim 20$ toroidal field coils) and high n (\dots , $n \gtrsim 10$, due to microturbulence). Magnetic fields in quasi-symmetric stellarators can be represented similarly.

Organization of paper: This theory-based topical overview paper concentrates on low and medium n perturbations. In order to elucidate the basics of 3D field effects, the first half of the paper (sections 2–5) assumes the 3D magnetic field Fourier coefficients δB_n and δB_N within the tokamak plasma are known. Plasma flows and the various toroidal torques that contribute to a comprehensive toroidal plasma rotation equation are discussed first. Next, the effects of non-resonant torques induced by non-resonant 3D fields with low n (global torques, section 3) and medium N (ripple drags, section 4), and finally low n resonant 3D fields (mode locking, section 5) are discussed. In these sections (2–5) it is implicitly assumed that these 3D fields are large enough so that the toroidal torques they induce dominate the toroidal plasma rotation equation and they can be examined in isolation. Then, in the second half of the paper (sections 6–9) the plasma responses and combined effects are discussed: resonant field amplification (RFA, section 6), instability effects (section 7), multiple resonant magnetic perturbations (section 8) and effects of toroidal rotation on plasma behavior (section 9). The final section summarizes the status of studies of 3D field effects on tokamak plasmas by discussing the results of the recent test blanket module (TBM) experiments and the possible implications of the present understanding of 3D field effects for ITER.

2. Plasma Toroidal Rotation And Transport Equations

Key equations: Transport equations for density, temperature and flows in tokamak plasmas that take account of 3D magnetic perturbation effects, including their effects on diamagnetic-level plasma flows, have been developed recently [3]–[6]. They go well beyond the 2D neoclassical-based transport equations [7, 8]. These developments build on the fluid moment approach to stellarator plasma transport in which flows within a flux surface are obtained first (see Refs. [9, 10] and references cited therein), before the self-consistent radial electric field and net cross-field “radial” transport fluxes are determined. But they go a step further by assuming the 3D magnetic perturbations $\delta\mathbf{B}$ are gyroradius small compared to the axisymmetric (or stellarator quasi-symmetric) magnetic field \mathbf{B}_0 . Then, various constraints on plasma flows are obtained on successive time scales [3]–[5]: 1) Radial ion force balance ($\nabla\psi \cdot [n_i q_i (\mathbf{E} + \mathbf{V}_i \times \mathbf{B}) - \nabla p_i] = 0$) enforced by compressional Alfvén waves on the μ s time scale yields

$$\begin{aligned} \mathbf{V}_i \cdot \nabla \zeta &= - \left(\frac{\partial \Phi_0}{\partial \psi} + \frac{1}{n_i q_i} \frac{\partial p_i}{\partial \psi} \right) + q \mathbf{V}_i \cdot \nabla \theta \\ \implies V_t &\simeq \frac{E_\rho}{B_p} - \frac{1}{n_i q_i B_p} \frac{dp_i}{d\rho} + \frac{B_t}{B_p} V_p. \end{aligned} \quad (2)$$

Thus, on the much longer transport time scale (typically \sim s) the plasma toroidal flow V_t is determined by a combination of $\mathbf{E} \times \mathbf{B}$, ion diamagnetic and poloidal ion flows. Here, $q(\psi)$ is the “safety factor” (slope of \mathbf{B}_0 on a ζ versus θ graph on the given ψ surface), B_p , B_t are the axisymmetric poloidal, toroidal magnetic field components and $\rho \equiv \sqrt{\psi_t / \pi B_{t0}}$ (units of m) is a toroidal-flux-based radial coordinate. 2) The poloidal flow V_p is damped to a primarily ion-temperature-gradient diamagnetic-type neoclassical flow [7, 8] on the ion collision time scale (\sim ms) plus possible microturbulence-induced effects specified in [4, 5]. Finally, 3) toroidal torque densities T_ζ caused by toroidal forces $\mathbf{F}_{\text{orces}}$ on a plasma species (subscript s with charge q_s) induce radial particle fluxes $\mathbf{\Gamma}_s \cdot \nabla \psi$:

$$T_\zeta \equiv \mathbf{e}_\zeta \cdot \mathbf{F}_{\text{orces}}, \quad \mathbf{e}_\zeta \cdot n_s \mathbf{V}_s \times \mathbf{B}_0 = \mathbf{\Gamma}_s \cdot \nabla \psi = -T_\zeta / q_s, \quad (3)$$

in which $\mathbf{e}_\zeta \equiv R^2 \nabla \zeta = R \hat{\mathbf{e}}_\zeta$ is the covariant toroidal angular vector. Setting the radial current caused by the sum of all the toroidal-torque-induced radial particle fluxes to zero (to obtain ambipolar transport) and neglecting magnetic flux transients yields [3, 4]:

$$\begin{aligned} \frac{\partial L_t}{\partial t} &\simeq - \underbrace{\langle \mathbf{e}_\zeta \cdot \nabla \cdot \vec{\pi}_{i\parallel}^{\leftrightarrow 3D} \rangle}_{\text{NTV from NR } \delta B} + \underbrace{\langle \mathbf{e}_\zeta \cdot \overline{\delta \mathbf{J} \times \delta \mathbf{B}} \rangle}_{\text{Resonant FEs}} \\ &\quad - \underbrace{\langle \mathbf{e}_\zeta \cdot \nabla \cdot \vec{\pi}_{i\perp}^{\leftrightarrow} \rangle}_{\text{cl, neo, paleo}} - \underbrace{\frac{1}{V'} \frac{\partial}{\partial \rho} (V' \Pi_{i\rho\zeta})}_{\text{Reynolds stress}} + \underbrace{\langle \mathbf{e}_\zeta \cdot \sum_s \bar{\mathbf{S}}_{sm} \rangle}_{\text{mom. sources}}. \end{aligned} \quad (4)$$

Here, the plasma angular momentum density L_t and toroidal rotation frequency Ω_t are

$$L_t \equiv \sum_{\text{ions}} m_i n_i \langle R^2 \mathbf{V}_i \cdot \nabla \zeta \rangle = I_t \Omega_t, \quad (5)$$

$$\Omega_t(\rho, t) \equiv \langle \mathbf{V} \cdot \nabla \zeta \rangle = L_t / I_t \sim V_t / R, \quad (6)$$

and $I_t \equiv \sum_{\text{ions}} m_i n_i \langle R^2 \rangle$ is the flux surface average (FSA) toroidal moment of inertia. Thus, (4) is the transport equation for the total plasma angular momentum density. Its L_t solution determines the FSA total plasma toroidal rotation frequency Ω_t . Each of the terms on the right of (4) can contribute significantly, or even become dominant, in specific tokamak operational scenarios, regimes and regions of the plasma. Using (2), this Ω_t determines the radial electric field for ambipolar radial density transport [3]–[5]:

$$E_\rho \equiv -|\nabla\rho| \frac{\partial\Phi_0}{\partial\rho} \simeq |\nabla\rho| \left[\Omega_t \psi' + \frac{1}{n_{i0} q_i} \frac{dp_i}{d\rho} - \frac{c_p}{q_i} \frac{dT_i}{d\rho} \right]. \quad (7)$$

Here, $\psi' \equiv d\psi/d\rho \simeq B_p R$, $c_p \equiv k_i \sim 1.17$ in $\sqrt{\epsilon} \ll 1$ ($\epsilon \equiv r/R_0 \ll 1$ is the inverse aspect ratio) neoclassical theory [7, 8], $V' \equiv \partial V/\partial\rho \propto \rho$ and $V(\rho, t)$ is the volume of the ρ flux surface.

Plasma torques: Terms on the right side of (4) represent [3]–[5] (in order of appearance) toroidal torque effects due to: non-resonant (NR) low and medium n 3D magnetic perturbation fields $\delta\mathbf{B}$ that induce neoclassical toroidal viscosity (NTV); low n resonant “field errors” (FEs); collision-induced classical, neoclassical and paleoclassical perpendicular viscosities; Reynolds (and Maxwell [4, 5]) stress due to high n microturbulence (see [11, 12]); and “external” toroidal momentum inputs. Relevant L_t boundary conditions and their effects plus integral forms of (4) are discussed in [6].

Ambipolar fluxes: In the comprehensive plasma toroidal rotation equation given by (4), radial particle fluxes induced by plasma toroidal torques are not individually ambipolar. Rather, only their sum is ambipolar. Thus, the requirement of ambipolar transport determines the plasma toroidal rotation (radial electric field). Since in tokamaks the dominant torques are on the ion species, the radial electric field is usually determined mainly by ion particle fluxes. This is called the “ion root” [of $\sum_s q_s \Gamma_s \cdot \nabla\psi = f(E_\rho) \rightarrow 0$] in stellarator transport theory. The net radial particle transport flux [4] is the sum of the intrinsically ambipolar collision-induced particle fluxes (classical plus neoclassical and paleoclassical) and non-ambipolar fluxes evaluated at the ambipolarity-enforcing radial electric field E_ρ (toroidal rotation frequency Ω_t). The radial energy transport fluxes induced by the low and medium n 3D field perturbations are small and perhaps negligible since they are order $\varrho_*^2 (B_t/B_p)^2$ smaller [3]–[5] than the usual axisymmetric collision- and microturbulence-induced energy transport fluxes. Here, $\varrho_* \equiv \varrho_i/a \ll 1$ is the usual dimensionless small ion gyroradius parameter.

3. Low n Non-resonant $\delta\mathbf{B}$ Torques (mainly induced by external coils)

Collision-induced toroidal torque: Using (2), the neoclassical toroidal viscous (NTV) torque induced by a single n non-resonant 3D perturbation [here $\delta B_n \simeq \sum_m \delta B_n(\psi, m)$] can be written in the generic form [3, 4]

$$- \langle \mathbf{e}_\zeta \cdot \nabla \cdot \vec{\pi}_{i\parallel}^{3D} \rangle \simeq - m_i n_i \mu_{\parallel} \left(\frac{\delta B_n}{B_0} \right)^2 \langle R^2 \rangle (\Omega_t - \Omega_*), \quad (8)$$

$$\Omega_* \simeq \frac{c_p + c_t}{q_i} \frac{dT_i}{d\psi_p} \sim \frac{1}{q_i R B_p} \frac{dT_i}{d\rho} < 0, \quad \text{offset frequency.} \quad (9)$$

Table 1. Particle diffusivities and NTV damping rates induced by ion drift effects.

Regime	f_Δ	$\Delta\rho$	$\frac{1}{\Delta t}$	$D_i \sim f_\Delta \frac{(\Delta\rho)^2}{\Delta t}$	$\mu_\parallel \sim D_i \frac{n^2 v_{Ti}^2 / R_0^2}{(v_d^{3D})^2}$	c_t
2D axisymmetric						
banana	$\sqrt{\epsilon}$	$\frac{q \varrho_i}{\sqrt{\epsilon}}$	$\frac{\nu_i}{\epsilon}$	$\nu_i \frac{q^2 \varrho_i^2}{\epsilon^{3/2}}$	0	–
3D trapped particles [$\nu_i < \epsilon^{3/2} \omega_{ti}$]						
$\frac{1}{\nu_i} < \frac{1}{\epsilon n \omega_E}$	$\sqrt{\epsilon}$	$v_d^{3D} \Delta t$	$\frac{\nu_i}{\epsilon}$	$\sqrt{\epsilon} \frac{(v_d^{3D})^2}{\nu_i / \epsilon}$	$\sqrt{\epsilon} \frac{n^2 v_{Ti}^2 / R_0^2}{\nu_i / \epsilon}$	2.4
$\sqrt{\frac{\nu_i}{\epsilon n \omega_E }} < 1$	$\sqrt{\epsilon} \left(\frac{\nu_i / \epsilon}{ n \omega_E } \right)^{1/2}$	$\frac{v_d^{3D}}{ n \omega_E }$	$ n \omega_E $	$\sqrt{\frac{\nu_i}{ n \omega_E }} \frac{(v_d^{3D})^2}{ n \omega_E }$	$\sqrt{\frac{\nu_i}{ n \omega_E }} \frac{n^2 v_{Ti}^2 / R_0^2}{ n \omega_E }$	0.34
$\omega_E \rightarrow 0$ (sbp)	$\sqrt{\epsilon} \left(\frac{\nu_i / \epsilon}{ n \omega_{d0} } \right)^{1/3}$	$v_d^{3D} \Delta t$	$\left(\frac{\nu_i n^2 \omega_{d0}^2}{\epsilon} \right)^{1/3}$	$\sqrt{\epsilon} \frac{(v_d^{3D})^2}{ n \omega_{d0} }$	$\sqrt{\epsilon} \frac{n^2 v_{Ti}^2 / R_0^2}{ n \omega_{d0} }$	0.0
ripple trapped	$\left(\frac{\delta B_N}{B_0} \right)^{1/2}$	$\frac{B_p}{B_0} v_{d0} \Delta t$	$\frac{\nu_i}{\delta B_N / B_0}$	$\left(\frac{\delta B_N}{B_0} \right)^{3/2} \frac{B_p^2}{B_0^2} \frac{v_{d0}^2}{\nu_i}$	$\frac{(B_p^2 / B_0^2) (v_{Ti}^2 / R_0^2)}{(\delta B_N / B_0)^{1/2} \nu_i}$	3.5
3D transit-resonant particles [$\omega_{d0} (\delta B_n / B_0)^{3/2} < \nu_i < \omega_{ti}$, TTMP]						
plateau	$\left(\frac{\nu_i R_0}{ n v_{Ti} } \right)^{1/3}$	$v_d^{3D} \Delta t$	$\left(\frac{\nu_i n^2 v_{Ti}^2}{R_0^2} \right)^{1/3}$	$\frac{(v_d^{3D})^2}{ n v_{Ti} / R_0}$	$ n (v_{Ti} / R_0)$	–0.5

This ion NTV torque damps toroidal rotation throughout the plasma toward an “offset” toroidal plasma rotation frequency Ω_* , which is in the counter-current direction, at a rate $\mu_\parallel (\delta B_n / B_0)^2$. All the seminal calculations of 3D-induced radial particle fluxes and NTV torques in tokamaks induced by δB_n in many possible asymptotic collisionality regimes have been made by Shaing and colleagues [9, 10], [13]–[18].

Radial particle fluxes, NTV: The non-ambipolar radial particle fluxes and resultant NTV torques can be understood in terms of collisional and precessional toroidal drift effects on radial drift motions induced by non-resonant 3D fields [3, 16]. Phenomenologically, the particle diffusion coefficient can be written as $D \sim f_\Delta (\Delta\rho)^2 / \Delta t$ in which f_Δ is the velocity space fraction of particles taking random radial steps $\Delta\rho$ at a rate $1/\Delta t$. The NTV damping frequency obtained from $q_i \langle \mathbf{T}_i \cdot \nabla \psi \rangle = -T_\zeta = \langle \mathbf{e}_\zeta \cdot \nabla \cdot \overleftrightarrow{\boldsymbol{\pi}}_{i\parallel}^{3D} \rangle$ is $\mu_\parallel (\delta B_n / B_0)^2 \sim (D_i / \varrho_i^2) (B_p / B_0)^2 = (D_i / v_{d0}^2) (v_{Ti}^2 / R_0^2)$ in which $\varrho_i \equiv v_{Ti} / \omega_{ci}$ is the ion gyroradius and $v_{d0} \equiv 2T_i / (q_i B_p R_0) = (B_0 / B_p) v_{Ti} (\varrho_i / R_0)$ with $v_{Ti} \equiv \sqrt{2T_i / m_i}$ is the reference (2D) gradient- B ion radial drift velocity [3, 13, 14] due to the toroidal curvature ($\simeq 1/R_0$) of the tokamak.

Scalings: Approximate dimensional forms of relevant ion drift effects and the induced ion diffusivities D_i , NTV damping frequencies μ_\parallel and 3D offset frequency coefficients c_t are shown in table 1. In 2D axisymmetric theory the centers of both electron and ion banana drift orbits remain on a flux surface. Thus, 2D neoclassical transport is ambipolar and causes no NTV torque [4]. (In the fluid approach the 2D torque T_ζ vanishes because there is no variation of $|\mathbf{B}|$ with ζ to impede flow in the

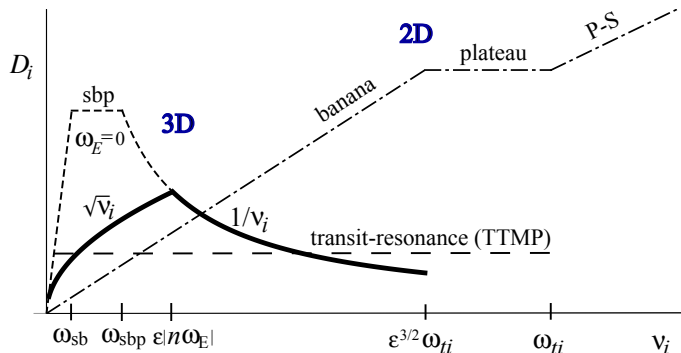


Figure 1. Ion collisionality regimes for **2D** and **3D** contributions to particle diffusivity $D_i \propto \text{NTV damping frequency } \mu_{\parallel}$. Transitions occur at key frequencies: ion transit $\omega_{ti} \equiv v_{Ti}/R_0q$, $\mathbf{E} \times \mathbf{B}$ -induced $\epsilon |n \omega_E|$, superbanana-plateau radial drift $\omega_{sbp} \equiv \epsilon |n| \omega_{d0}$ and superbanana $\omega_{sb} \equiv \epsilon^{-1/2} (\delta B_n/B_0)^{3/2} (|n| \omega_{d0})$. The 3D D_i and μ_{\parallel} become large (sbp regime) when $\omega_E \rightarrow 0$ (short dashes curve) where the radial motions of ions are limited by ω_{d0} instead of ω_E .

toroidal direction.) The 3D fields introduce radial drifts of the centers of trapped-ion banana orbits (“banana-drifts” [19]) with drift velocity

$$v_d^{3D} \equiv n (\delta B_n/B_0) v_{d0}, \quad \text{3D radial drift speed.} \quad (10)$$

Only trapped particles are involved in banana-drift effects. In the $1/\nu$ regime in table 1 radial excursions of the banana centers are limited by collisions. In the $\sqrt{\nu}$ regime they are limited by boundary layer effects on barely trapped particles. (The $\sqrt{\nu}$ regime includes and mostly supersedes [14] the original ν regime [13]. Order unity logarithmic factors in [14] are neglected here and in figure 1.) In table 1 and figure 1

$$\omega_E \equiv \frac{\partial \Phi_0}{\partial \psi} = -\frac{1}{n_i q_i} \frac{dp_i}{d\psi} + \frac{c_p}{q_i} \frac{dT_i}{d\psi} - \Omega_t \simeq -\frac{E_\rho}{RB_p} \quad (11)$$

is the $\mathbf{E} \times \mathbf{B}$ -induced toroidal precession drift frequency [13] that is specified in terms of the plasma toroidal rotation frequency Ω_t by (7). When $\omega_E(\Omega_t) \rightarrow 0$, radial “superbanana plateau” (sbp) drift excursions are limited by the precessional toroidal drift induced by the reference (2D) gradient- B drift frequency $\omega_{d0} \equiv v_{d0}/R_0$. Ripple-trapping effects [17] are discussed in the next section. Finally, 3D fields produce transit (and bounce, drift) resonances that induce plateau-like diffusion [10], which is highlighted in [20, 21] and comprehensively evaluated in [22]. This last effect is analogous to transit-time-magnetic-pumping (TTMP) effects by RF waves [23]. Equation (40) in [10] provides a simple estimate of it for rippled tokamaks.

Collisionality regimes: The applicable ν_i ranges for the typically most important $1/\nu$, $\sqrt{\nu}$ and superbanana-plateau 3D trapped-ion transport are illustrated schematically in figure 1. Also shown are those for the standard 2D axisymmetric (banana, plateau and Pfirsch-Schlüter), 3D plateau (TTMP) and very low collisionality 3D superbanana [16] transport. Since the 3D contributions from trapped ($1/\nu$, $\sqrt{\nu}$ and sbp) and transit-resonant particles (TTMP) arise from different regions of velocity space, at a given ion collision frequency their effects are additive. Note that when $\epsilon |n \omega_E(\Omega_t)|$

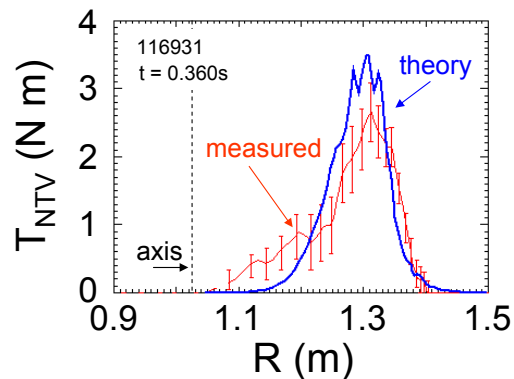


Figure 2. NSTX experimental test [32] of the spatial profile and magnitude of NTV-induced torque $T_{\text{NTV}} \equiv \langle \mathbf{e}_\zeta \cdot \nabla \cdot \vec{\pi}_{i\parallel}^{\text{3D}} \rangle / n_i$ (theory) and $T_{\text{NTV}} \equiv \delta\rho V' d(I_t \Omega_t) / dt$ (measured, for annulus width $\delta\rho$) induced by an applied $n=3$ non-resonant 3D field.

becomes smaller than $\omega_{\text{sbp}} \equiv \epsilon |n\omega_{d0}|$ the diffusivity D_i and viscous damping frequency μ_{\parallel} are predicted to become large. Approximate multi-collisionality trapped-particle NTV torque formulas that include the radial force balance constraint and diamagnetic-level poloidal flow effects have recently been proposed [24, 16, 25]. If ripple-trapping occurs, as discussed in the next section, its effects [17] should also be added.

Initial experimental tests: Reduction of Ω_t induced by externally imposed non-resonant ($m/n=1/3$) 3D fields was first observed experimentally on DIII-D [26] where it was compared with an adaptation of TTMP RF theory [23]. Magnetic braking induced by TTMP effects of field errors was explored for JET plasmas [27]. Reduction of the NTV damping rate with the degree of stellarator quasi-helical symmetry has been demonstrated on HSX [28, 29]. NTV effects have been observed extensively in NSTX [30]–[33]. Figures 2 and 3 show the first detailed comparisons of NTV theory (in the $1/\nu$ regime) with toroidal torque data from NSTX [32]; this pioneering paper introduced the “neoclassical toroidal viscosity” (NTV) terminology. In retrospect, the good agreement shown in figures 2, 3 is a bit fortuitous — because later theory developments showed the hotter parts of these NSTX plasmas were likely in the $\sqrt{\nu}$ regime where the NTV torque is somewhat smaller, but the competing “Lagrangian” effect (see section 6) induced by the plasma response fluid motion $\boldsymbol{\xi}$, which increases δB_n via variations along $\mathbf{B}_0(\mathbf{x}+\boldsymbol{\xi})$, was not included. Recent estimates of $n=1$ NTV effects in JET [34] found them to be too small; however neither the important resonant field amplification (RFA) effects (see figure 3) nor Lagrangian effects (see section 6) were included in those studies.

Experimental tests of offset: Damping of Ω_t by NTV to the offset frequency Ω_* in (8), first highlighted in [35], has been convincingly demonstrated in DIII-D using a $n=3$ non-resonant magnetic field (NMRF) [36, 37, 38], as shown in figure 4. These papers introduced the “offset” rotation frequency terminology. These studies also showed [37] that the NTV torque was proportional to the square of the I-coil current and hence to δB_n^2 . The offset frequency Ω_* defined in (9) is caused by

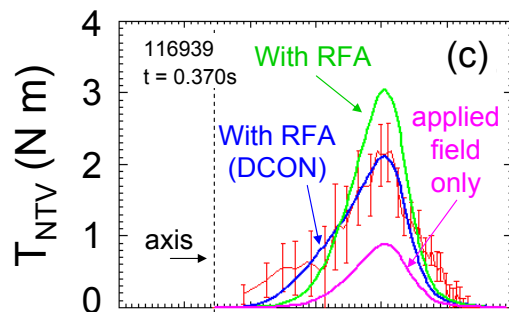


Figure 3. NSTX experimental test [32] of the NTV torque shows for $n = 1$ δB_n resonant field amplification (RFA) effects are needed to obtain agreement with NTV theory. For the radial scale see figure 2.

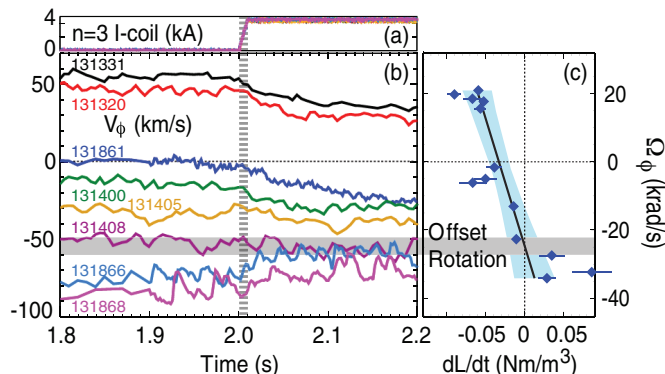


Figure 4. DIII-D experiments validated [36, 37] the NTV-induced damping/braking to the offset rotation frequency Ω_* , as implied by the NTV formula in (8).

superthermal ions diffusing radially more rapidly than thermal ions. Thus, a reduced toroidal rotation frequency Ω_t is required to obtain the same NTV torque and hence ambipolar radial particle transport compared to the case where T_i is spatially constant. Alternatively, from (2) the offset Ω_* represents the decrease in E_ρ needed to hold back more thermal ions to obtain ambipolar transport when $dT_i/d\rho < 0$. In addition, rotating magnetohydrodynamic (MHD)-type modes in MAST [39] have been shown to induce torque and offset frequency effects consistent with NTV theory.

Peak NTV: The E_ρ -induced drift frequency ω_E varies with Ω_t , as indicated in (11). Thus, the NTV damping frequency $\mu_{\parallel}(\nu_i, \omega_E)$ and torque vary nonlinearly with ω_E (or Ω_t). They peak where $\omega_E \rightarrow 0$, as indicated by the dashed curve in figure 1. This key effect has been demonstrated recently on DIII-D [40, 41, 42], for a non-resonant $n = 3$ field at a β_N well below the ideal MHD no-wall stability limit, as shown in figure 5.

Status: Recent tokamak experiments have exploited NTV effects by applying $\delta B_n/B_0 \sim 10^{-3}$ low n non-resonant external magnetic perturbations to produce new regimes of QH-mode operation [43] and reduce resonant field error effects [44]. The

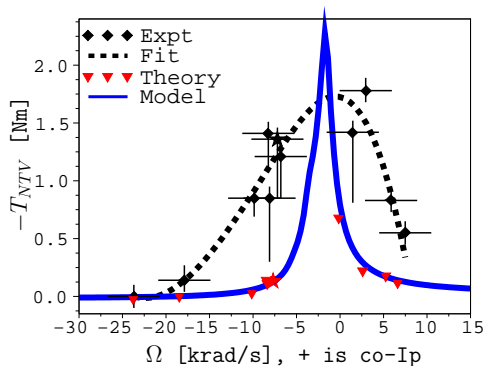


Figure 5. DIII-D experiments validated [40, 41, 42] NTV peak caused by $\mu_{\parallel}(\nu_i, \omega_E)$ occurs where $\omega_E \simeq 0$ at which $\Omega_t \simeq -2$ krad/s.

composite of the various experimental tests and uses of the NTV torque validate qualitatively and to some degree quantitatively the neoclassical-based theory of the toroidal torque induced by the effects of externally applied low n non-resonant 3D fields.

4. Medium n Non-resonant δB Torques (due to toroidal field ripple)

Physical effects: The magnetic field ripple caused by the finite number N of toroidal field coils (typically $N = 18$ – 32 , with $\delta B_N/B_0 \lesssim 10^{-2}$) induces various types of 3D NTV and ion direct loss effects, which are additive. The ripple-induced 3D trapped-particle contributions in table 1 are usually in the $\sqrt{\nu}$ regime because $n \rightarrow N$ is large so typically $\nu_i < \epsilon |N\omega_E|$. The 3D transit-resonance (TTMP) effects [10, 20, 22] can cause the dominant ripple effect. In addition, low collisionality ions with $\nu_i < (\delta B_N/B_0)^{1/2} N\omega_{ti}$ can be trapped in ripples (if $\epsilon |\sin \theta| < Nq\delta$ [17]) causing ions to drift radially inducing a radial ion particle flux and hence NTV torque that scales as $(\delta B_n/B_0)^{3/2}$ [3, 17], as indicated in the “ripple trapped” row of table 1. Finally, near the plasma edge superthermal ions or NBI-produced fast ions can be ripple trapped or have up-down asymmetric banana drift orbits and drift out of the plasma. This “direct loss” FSA radial ion current $\langle \mathbf{J}_{\text{dl}} \cdot \nabla \psi_p \rangle$ has no direct effect on the plasma. However, it induces a radial “return current” in the plasma to preserve quasineutrality [45, 4]. When this radially inward (negative) plasma return current is crossed with \mathbf{B}_p , it induces a toroidal torque on the edge plasma in the counter-current direction [45]. This effect is represented in (4) by a momentum sink (see section V of [4]) $\langle \mathbf{e}_\zeta \cdot \bar{\mathbf{S}}_m \rangle = -\langle \mathbf{J}_{\text{dl}} \cdot \nabla \psi_p \rangle$ induced by the plasma response to the \mathbf{J}_{dl} . Thus, ripple-induced direct loss and NTV effects both decrease a positive plasma toroidal rotation frequency Ω_t . NTV effects damp it toward the offset rotation frequency Ω_* in the counter-current direction.

Experimental results: A reduction in plasma toroidal rotation induced by ripple effects was first observed in ISX-B where adjacent toroidal field coils were de-energized to produce an $N = 9$ coil system with an edge ripple of $\delta \equiv \delta B_N/B_0 \sim 10\%$ [46]. Experiments in JT-60U L-mode plasmas with and without ferritic steel tiles (FSTs) to

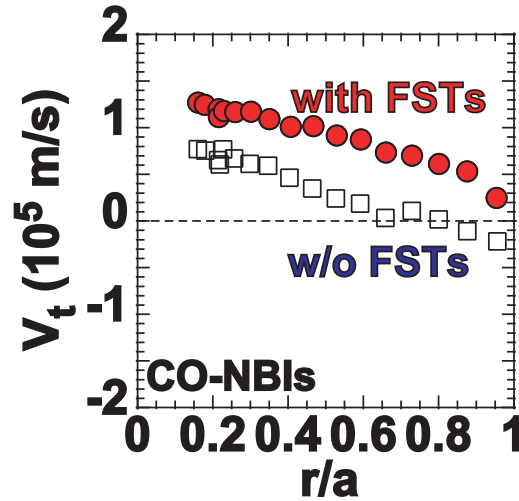


Figure 6. Toroidal plasma flow decreases as field ripple in JT-60U increases from 1% (with FSTs) to 2% without (w/o) FSTs [47].

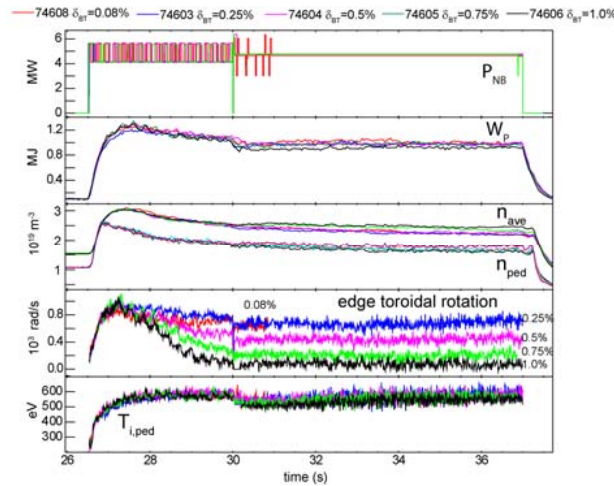


Figure 7. Toroidal plasma rotation decreases monotonically with increasing field ripple (% #s at right of 4th panel) in edge of JET [50].

reduce the $N=18$ field ripple (edge δ was reduced from 2% to 1%) observed a decrease in plasma toroidal flow toward the counter-current direction for the higher ripple case [47], as shown in figure 6. This result agrees in the edge with theoretical modeling of the effects of the edge ripple-induced ion direct loss current effect [48]. Also, the decrease in edge toroidal flow in JT-60U increases monotonically with increasing perpendicular NBI power which increases the edge ion direct loss current [47]. Recently, variable-ripple experiments have been performed by changing the current in adjacent (even/odd) toroidal field coils. The edge ripple in the $N=24$ JET configuration [49, 50] was varied from 0.08% to 1% and from 0.8% to 7% in Tore Supra experiments [51]. The edge Ω_t decreased monotonically as ripple was increased [49, 50], as shown for JET in figure

7. All other plasma and pedestal profiles in JET were essentially unchanged as long as a ripple-induced “density pump-out” at the edge was compensated for by increased gas puffing to keep the overall plasma density constant [50, 52]. The differing ripple magnitudes between the JT-60U and JET devices had previously been identified [53] as the cause of slightly smaller pedestal pressures in JT-60U. Finally, analysis of the decrease in the edge Ω_t toward the counter-current direction in JT-60U has been shown [54] to be proportional to $dT_i/d\rho$, which could be caused by the NTV Ω_* offset frequency.

Status: Decreases in edge Ω_t toward the counter-current direction caused by ripple-induced ion direct losses are in good agreement with predictions [48, 55]. Modeling of ripple effects has concentrated on effects of the FSA ion ion loss current $\langle \mathbf{J}_{\text{dl}} \cdot \nabla \psi_p \rangle$ and used phenomenological-type models [19] for banana-drift effects [48, 55] without taking account of self-consistent radial electric field effects (i.e., the Ω_t or ω_E dependence of the ripple-induced non-ambipolar ion radial particle fluxes). Modeling the full $\Omega_t(\rho)$ profile in rippled tokamaks when both NTV (from trapped and transit-resonant particles [13]–[18]) and edge ion direct loss effects are present requires self-consistent calculations using (4) and (8). Particularly important would be a modeling confirmation of the offset frequency Ω_* (< 0) effect in rippled tokamaks. Ripple-type effects caused by Test Blanket Modules (TBMs) being proposed for ITER are discussed in the final section.

5. Low n Resonant $\delta\mathbf{B}$ Torques (mode locking from field errors)

Mode locking physics: Field errors (FEs) often introduce low n (e.g., $n = 1$) magnetic perturbations that are resonant with field lines in the plasma where $q(\rho_{m/n}) = m/n$. Resonant 3D perturbations can also be intentionally applied. A resonant 3D field can slow toroidal plasma rotation at the resonant surface $\rho_{m/n}$, cause magnetic reconnection there, form a growing magnetic island, induce “locked” (to the wall) magnetohydrodynamic (MHD) modes [56, 57] and possibly lead to plasma disruptions.

Ideal MHD model: The first order magnetic field perturbation induced by a plasma displacement $\boldsymbol{\xi}$ is given by $\delta\mathbf{B} = \nabla \times (\boldsymbol{\xi} \times \mathbf{B}_0) = (\mathbf{B}_0 \cdot \nabla)\boldsymbol{\xi} - \mathbf{B}_0(\nabla \cdot \boldsymbol{\xi})$ in ideal MHD. Thus, the magnetic field advects “non-resonantly” with the plasma fluid, which yields the “frozen flux theorem.” Hence, for ideal MHD it can be shown [58, 59] that there is no FSA toroidal torque on the plasma, i.e., $\langle \mathbf{e}_\zeta \cdot \overline{\delta\mathbf{J} \times \delta\mathbf{B}} \rangle = 0$. Behavior near a rational surface is singular [58, 59]. This occurs because the magnetic field cannot advect with $\boldsymbol{\xi}$ there since the radial component $\delta B_\rho \equiv \delta\mathbf{B} \cdot \nabla \rho = (\mathbf{B}_0 \cdot \nabla)(\boldsymbol{\xi} \cdot \nabla \rho)$ must vanish at rational (resonant) surfaces in the plasma because $\mathbf{B}_0 \cdot \nabla \sim i(m - nq)/R_0q \rightarrow 0$ for $q(\rho_{m/n}) = m/n$. To satisfy this ideal MHD constraint that $\delta B_{\rho_{m/n}}(\rho) \equiv \nabla \rho \cdot \delta\mathbf{B}_{m/n}$ vanish at $\rho_{m/n}$, a delta-function “shielding current” $\delta\mathbf{J}_{\parallel m/n}$ is introduced at each m/n rational surface in response to an externally imposed $\delta\mathbf{B}_{m/n}$. Even with this delta-function shielding current the resonant FSA toroidal torque $\langle \mathbf{e}_\zeta \cdot \overline{\delta\mathbf{J}_{\parallel m/n} \times \delta\mathbf{B}_{m/n}} \rangle = (d\psi/d\rho) \langle \overline{\delta\mathbf{J}_{\parallel m/n} \delta B_{\rho_{m/n}}/B_0} \rangle$ vanishes [59]. Thus, in the purely ideal MHD model an externally imposed 3D field induces non-resonant $\delta\mathbf{B}$ and $\delta\mathbf{J}$ responses in the plasma but exerts no toroidal torque on the plasma [58, 59, 60].

Nonideal MHD: Dissipative, nonideal (e.g., resistive or even continuum Landau damping [59]) effects allow the shielding current $\delta\mathbf{J}_{\parallel m/n}$ induced by a resonant 3D field to cause a nonzero $\delta B_{\rho m/n}(\rho_{m/n})$. The resultant $\delta\mathbf{J}_{\parallel m/n}$ occurs within a thin “singular” layer of width δ_S around the low order rational surface $\rho_{m/n}$ [58, 60]. Thus, nonideal effects produce a local Maxwell-stress-induced FSA toroidal plasma torque density. For a cylindrical model and representing the thin resistive singular layer at $\rho_{m/n}$ with a δ -function, this FSA toroidal torque can be written in the form

$$\begin{aligned} \langle \mathbf{e}_\zeta \cdot \overline{\delta\mathbf{J}_{\parallel m/n} \times \delta\mathbf{B}_{m/n}} \rangle &\simeq -m_i n_i (4nc_A^2) \left(\frac{\delta B_{\rho m/n}^{\text{vac}}}{B_0} \right)^2 \\ &\times \left[\frac{(-\omega\tau_S)}{(-\Delta')^2 + (-\omega\tau_S)^2} \right] \frac{V \delta(\rho - \rho_{m/n})}{V'}. \end{aligned} \quad (12)$$

Here, $c_A \equiv B_0/\sqrt{\mu_0 m_i n_i}$ is the Alfvén speed, $\delta B_{\rho m/n}^{\text{vac}} \equiv \nabla\rho \cdot \delta\mathbf{B}_{m/n}^{\text{vac}}$ is the radial component of the m/n Fourier coefficient of the 3D vacuum field perturbation $\delta\mathbf{B}^{\text{vac}}$, $\omega \equiv \mathbf{k} \cdot \mathbf{V}_i = -n\Omega_t + m\langle \mathbf{V}_i \cdot \nabla\theta \rangle = n[\omega_E + (1/n_i q_i)(dp_i/d\psi)]$ is the resistive MHD plasma-flow-induced response frequency in the laboratory frame, $\tau_S = \delta_S \rho_{m/n}/(\eta/\mu_0) \sim 10^{-2}$ – 10^{-3} s is the resistivity-induced singular-layer diffusion time and Δ' is the tearing instability index (< 0 for stability), which can be influenced by an externally applied field error [61]. In this resistive singular layer model [58, 60] the magnetic field perturbation at the rational surface is the vacuum $\delta B_{\rho m/n}^{\text{vac}}$ multiplied by the ω -dependent term in square brackets on the second line of (12).

Resonant field effects: The radially localized torque density in (12) tries to stop plasma toroidal rotation at the rational surface induced by the momentum source $\langle \mathbf{e}_\zeta \cdot \sum_s \bar{\mathbf{S}}_{sm} \rangle$. However, radial diffusion of the toroidal flow by the collision- and microturbulence-induced perpendicular viscous diffusivity $\chi_{\zeta i}$ limits the jump in the radial derivative of Ω_t in the vicinity of the rational surface [58, 60, 62]. The ω (and hence Ω_t , ω_E -dependent) factor in square brackets in (12) represents the nonideal (resistive) singular layer effects. Its $\omega/(\omega^2 + \omega_0^2)$ resonant frequency dependence causes the plasma response to be analogous to induction motor responses to a rotating magnetic field [58, 60]. For $|\omega\tau_S| \gg 1$ plasma toroidal rotation and $\chi_{\zeta i}$ inhibit penetration of $\delta B_{\rho m/n}$ into the singular layer by producing an ideal MHD-type “superconducting plasma” shielding response for $\rho \leq \rho_{m/n}$ [57, 58, 60]. That is, in a cylindrical model it causes $\delta B_{\rho m/n}^{\text{vac}}$ to vanish for $\rho \leq \rho_{m/n}$. However, when $\delta B_{\rho m/n}^{\text{vac}}$ is large enough to reduce $|\omega\tau_S|$ to about $-\Delta' \sim 2m$, the “penetration threshold” is exceeded (e.g., for $\delta B_{\rho_{2/1}}^{\text{vac}}/B_0 \gtrsim 10^{-4}$ [56]–[69]), $\Omega_t(\rho_{m/n})$ is no longer restrained by $\chi_{\zeta i}$ effects and plasma rotation no longer “shields” or “screens” out the resonant torque. Then, the solution of (4) bifurcates (typically in a few ms) to a state where plasma toroidal rotation vanishes at $\rho_{m/n}$, magnetic reconnection occurs there and a growing m/n locked mode magnetic island is induced, which often leads to a plasma disruption.

Recent theory developments: More physically relevant (mainly Visco-Resistive regime) two-fluid singular layer effects have recently been developed [62]. When they are included, the resonant frequency behavior in (12) occurs where the frequency ω is

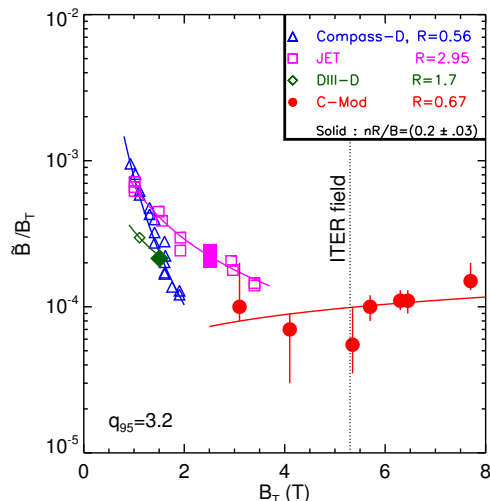


Figure 8. Relative threshold for the 2/1 magnetic perturbation ($\propto n_e R_0$ for solid points, $q_{95} \simeq 3.2$) above which locked modes occur [65].

equal to either the electron or ion diamagnetic drift frequencies $\omega_{*e,i} \equiv \mathbf{k} \cdot \mathbf{V}_{*e,i}$. In a cold ion limit (i.e., assuming $T_i \rightarrow 0$) there is only a single frequency resonance which occurs where $\omega - \omega_{*e} = 0$ [63], i.e., where $n\Omega_t = -\omega_{*e} (> 0)$, $\mathbf{V}_{\mathbf{E} \times \mathbf{B}} = \mathbf{V}_{*e}$ in this model. Including physically relevant $T_i \neq 0$ effects adds a poloidal ion flow frequency shift and ion diamagnetic frequency effects that depend on the specific parameter regime [62]. While the precise Ω_t at which the field-error-induced torque like that in (12) is maximum is uncertain, it is of the order of the electron or ion diamagnetic flow frequencies and relatively small (~ 10 krad/s in present experiments). The NTV effects add a global torque effect that attempts to keep the plasma rotating at the rate Ω_* [35, 64]; they amplify the viscosity-induced plasma rotation shielding effects by a factor $\Gamma_s \equiv [\rho_m^2/n\mu_{\parallel}(\delta B_n/B_0)^2/\chi_{\zeta i}]^{1/2}$, when it exceeds unity. Finally, and most critically for mode-locking thresholds at fusion-relevant $\beta \equiv P/(B_0^2/2\mu_0)$ values, resonant field amplification (RFA), mainly via weakly damped MHD kink-type $n=1$ resonant plasma responses to externally applied perturbations, are being explored. RFA is discussed in the next section.

Recent experimental studies, status: Field error locking results from many tokamaks are summarized empirically in [65], as shown in figure 8. The field error mode-locking threshold scales primarily about linearly with plasma density in ohmic-level plasmas. The recent NTV-influenced mode-locking theory [35, 64] agrees most closely [64] with this scaling. However, detailed quantitative comparisons with theory require knowledge of the magnitude and scaling of the perpendicular ion momentum diffusivity $\chi_{\zeta i}$ and remain to be made. Recent detailed experimental studies of field error mode-locking thresholds obtained with a mix of intrinsic field errors and external fields applied to compensate them found that MHD-like plasma response effects [66] must be included [67]–[69]. That is, the torque in (12) depends on the plasma-response

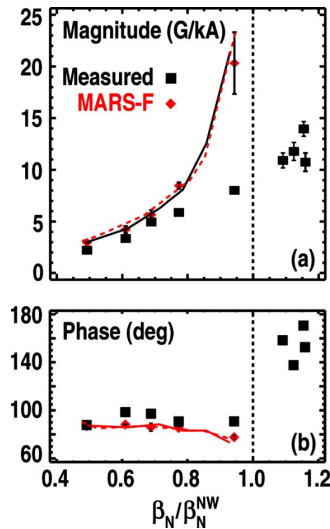


Figure 9. a) The magnitude of the $n=1$ plasma response (black squares), measured by poloidal field probes inside the vacuum vessel wall on the DIII-D outer midplane, increases about linearly with β_N . An ideal MHD MARS-F calculation [73] (red diamonds) of the probe measurement agrees well with the measurements below 80% of the beta no-wall limit. b) The corresponding $n=1$ plasma response phases.

resonant $\delta B_{\rho m/n}^{\text{plasma}}$ near the rational surface instead of just the vacuum field resonant field component $\delta B_{\rho m/n}^{\text{vac}}$ there. The resonant field amplification (RFA) scales approximately linearly with β at high β [67, 68], as shown in figure 9. Hence “dynamic” field error compensation is usually needed for optimum error field control as β increases [69]. Also, non-resonant NTV is being used to control and compensate for field error effects on Ω_t [44, 69]. Finally, a combination of NTV and phase-locked ECCD have been used to cause locked modes to “commit suicide” and not evolve into plasma disruptions [70].

6. Plasma Resonant Field Amplification (RFA) Of δB

Multiple components: Externally applied 3D magnetic perturbations usually have many m, n Fourier components whose NTV, ripple-trapping and resonant FE effects should be summed in (4)–(12). However, the $\delta B_n(\psi, m)$ and $\delta B_{\rho m/n}$ amplitudes and phases $\varphi_{m,n}$ within the plasma need to be evaluated including plasma responses, i.e., not be vacuum values. Plasma responses to non-resonant fields are usually modest, except for β values near or above the no-wall limit [32, 37]. But for $n=1$ resonant fields, figures 3 and 9 have already indicated the importance of plasma response effects for obtaining the correct magnitude of NTV and $\delta B_{\rho m/n}$ effects.

Plasma response effects: The plasma can amplify externally applied 3D resonant components of $\delta \mathbf{B}$ within the plasma [71, 72]. The amplification is analogous to the driven response of a weakly damped oscillator. It is strongest if the $\delta \mathbf{B}$ components couple to weakly damped MHD-type global eigenmodes [73]. The “least stable” (smallest damping rate) MHD-type eigenmodes are usually $n=1$ kink-type modes that

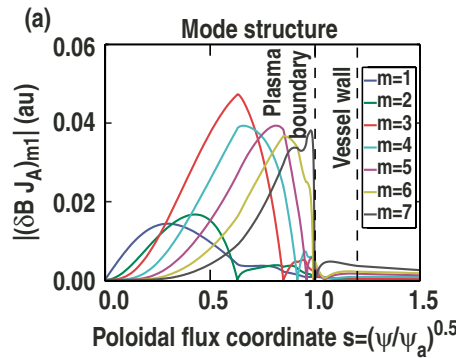


Figure 10. Poloidal mode spectrum of $\delta B_{\rho m/1}$ from nonideal MARS-F [73] calculation for an unstable RWM in DIII-D [67] with $q_{95} \simeq 5$.

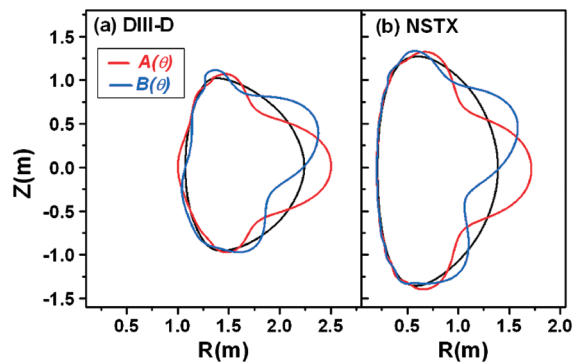


Figure 11. Distributions of external 3D fields from IPEC [75] that maximize the total resonant fields on rational surfaces [66] in a) DIII-D and b) NSTX.

progressively “balloon” on the outboard side of the plasma cross section as β increases. Non-resonant fields with $n > 1$ or $m/n < 0$ don’t naturally couple to $n = 1$ kink-type eigenmodes. Thus, usually they are not significantly modified by plasma responses [74]. However, externally applied 3D fields that can couple to the least stable $n = 1$ kink-type MHD eigenmodes can amplify the $m/1$ magnetic field components within the plasma. Figure 10 shows the various m components of a representative kink-type $n = 1$ resistive wall mode (RWM) [68], whose 3D field components are similar to those for a $n = 1$ weakly damped kink mode. Since at the plasma edge the dominant poloidal mode number m of a global $n = 1$ kink-type eigenmode is $m \gtrsim q \gtrsim q_{95}$, $m/1$ components of an externally applied $\delta \mathbf{B}$ that couple most strongly [67, 68] are those which are localized on the outboard midplane (where the straight-field-line θ coordinate values are most widely spaced) to $\Delta\theta \sim 2\pi/m$, as indicated in figure 11 [66, 75]. That is, $n = 1$ external field error (or error compensation) 3D components that cause the largest $\delta B_{\rho m/n}$ responses at the $m/n = 2/1, 3/1$ resonant surfaces within the plasma are those [67, 68] which are field-line-pitch-resonant with the external or edge $n = 1$ global kink eigenmode components with $m \gtrsim q \gtrsim q_{95}$ there.

Ideal MHD theory and modeling of plasma responses: Section 5 discussed responses to resonant field errors. As noted there, in the ideal MHD model when an external 3D m/n resonant perturbation is applied to a rapidly rotating (i.e., $|\omega\tau_S| \gg 1$) plasma, a delta-function “shielding current” $\delta J_{\parallel m/n}$ must be introduced to satisfy the ideal MHD constraint that $\delta B_{\rho m/n}(\rho_{m/n}) = 0$ [71]. This generic procedure was used in the calculation of resonant field amplification (RFA) effects in the original NTV explorations on NSTX [32], as shown in figure 3. An innovative ideal MHD perturbed equilibrium code (IPEC [66, 75]) has been developed to implement this procedure using the linear ideal MHD stability DCON code [76]. It was used to produce the field error sensitivities shown in figure 11. The combination of the shielding current $\delta J_{\parallel m/n}$ and the (magnetically reconnected) $\delta B_{\rho m/n}^{\text{IPEC}}$ this sheet current would produce if it were relaxed by nonideal MHD effects has been used [66] to very approximately estimate the resonant toroidal torque $\langle \mathbf{e}_\zeta \cdot \overline{\delta \mathbf{J}_{\parallel m/n} \times \delta \mathbf{B}_{\rho m/n}} \rangle$ by replacing the $\delta B_{\rho m/n}^{\text{vac}}$ in (12) with $\delta B_{\rho m/n}^{\text{IPEC}}$ and using two-fluid layer physics [62, 64] for the term in square brackets in (12). This procedure provided encouraging explanations [75] for field error compensation effects in DIII-D (via externally applied 3D fields) and NSTX (via phasing of external correction coils). However, while qualitative trends are captured, subsequent more precise evaluations have been less conclusive [21].

Nonideal singular layers: Figure 9 shows that while the resonant field amplification (RFA) of $\delta B_{\rho m/n}$ increases about linearly with β well below the no-wall limit, the ideal MHD response (calculated in figure 9 with MARS-F [73]) predicts too large a plasma response as β increases toward the no-wall ideal MHD stability limit. To avoid non-physical singularities in the response at the no-wall limit it is critical [78] to calculate the torque on the plasma (in its nonideal layer) rather than its opposite which is the torque on the wall and error field structure as in the ideal MHD models. This is particularly important in assessing the possible effects [79] of a flowing liquid metal wall at the ideal MHD no-wall limit [80]. Nonideal effects in the singular layer are critical for calculating rotating plasma torque responses such as that shown in figure 10 and in achieving stable plasmas above the ideal no-wall limit. Also, global kinetic response resistive wall mode physics can become important there (see section 7). The resonant toroidal torque $\langle \mathbf{e}_\zeta \cdot \overline{\delta \mathbf{J}_{\parallel m/n} \times \delta \mathbf{B}_{\rho m/n}} \rangle$ can be evaluated rigorously [74] using a linear code such as MARS-F [73]. When nonideal MHD effects are included [74, 77], the singular layer effects and the reconnected resonant magnetic field $\delta B_{\rho m/n}^{\text{plasma}}$ in the layer can be calculated self-consistently, unlike how its form is assumed for IPEC estimates [21]. More generally and comprehensively, nonlinear 3D initial value codes such as M3D [81], NIMROD [82] or reduced MHD codes (BOUT++ [77] or JOEK [83]) could calculate the resonant toroidal torque and also explore the dynamics of the field-error-induced mode locking process. To date these codes only use resistive MHD or limited two-fluid nonideal MHD layer physics models. The neoclassical MHD inertia effects [84, 85] should also be included. Non-resonant 3D field components $\delta B_n(\psi, m)$ are also generated in response to edge-resonant $n = 1$ field errors and can cause NTV “global” toroidal flow damping effects in conjunction with resonant $\delta B_{\rho m/n}^{\text{plasma}}$ effects [67, 68, 69, 21].

Lagrangian effects on δB_n : Resonant field amplification of $\delta \mathbf{B}$ within the plasma also changes [13] the δB_n Fourier coefficients in the evaluation of the NTV torque in (8). In the presence of a plasma fluid displacement $\boldsymbol{\xi}$, the lowest order magnetic field is changed to $\mathbf{B}_0(\mathbf{x} + \boldsymbol{\xi})$. The difference of this $\mathbf{B}_0(\mathbf{x} + \boldsymbol{\xi})$ from the axisymmetric field $\mathbf{B}_0(\mathbf{x})$ is a ‘‘Lagrangian’’ magnetic field perturbation $\delta \mathbf{B}^L = \mathbf{B}_0(\mathbf{x} + \boldsymbol{\xi}) - \mathbf{B}_0(\mathbf{x}) = (\boldsymbol{\xi} \cdot \nabla) \mathbf{B}_0 + \mathcal{O}(\xi^2)$. The total first order magnetic perturbation $\delta \mathbf{B}$ is the sum of two linear perturbations: the first order part of the Lagrangian perturbation $\delta \mathbf{B}^L$ plus the usual Eulerian $\delta \mathbf{B}^E$ due to variations along the lowest order axisymmetric magnetic field \mathbf{B}_0 induced directly by the $\delta \mathbf{B}(\mathbf{x})$ which includes the plasma response. The parallel component of $\delta \mathbf{B}^L$ can be written as $\delta B_{\parallel}^L = (\mathbf{B}_0/B_0) \cdot (\boldsymbol{\xi} \cdot \nabla) \mathbf{B}_0 + \mathcal{O}(\xi^2) = (\boldsymbol{\xi} \cdot \nabla) B_0 + \mathcal{O}(\xi^2)$. Thus, in the presence of a plasma fluid displacement $\boldsymbol{\xi}$ the total $\delta B_n(\psi, m)$ coefficients are the θ, ζ Fourier coefficients of $\delta B_{\parallel} \equiv \delta B_{\parallel}^E + \delta B_{\parallel}^L = (\mathbf{B}_0/B_0) \cdot \delta \mathbf{B} + (\boldsymbol{\xi} \cdot \nabla) B_0$.

Experimental studies, status: The first experimental indications of plasma response effects were seen in 1992 in the β dependence of the mode locking thresholds in DIII-D [86]. Resonant field amplification (RFA) was later observed above the no-wall β limit [87, 88, 89] and shown to be caused by a marginally stable $n = 1$ RWM [89]. More recently, RWM-induced RFA proportional to β has been observed along with NTV damping effects in NSTX [31], analogous to the results shown in figure 9. The IPEC studies [66, 21] of plasma response effects induced by externally applied 3D fields to compensate for field errors were instrumental in demonstrating the importance of these effects. Understanding of plasma response effects and correction of both $n = 1$ and $n = 3$ intrinsic field errors have led to sustained high plasma toroidal rotation and record plasma durations free of MHD activity in NSTX [69]. The IPEC plasma response studies [66, 75, 21] have also provided the impetus for studies using MARS-F and nonlinear initial value codes of the plasma response effects including nonideal MHD layer physics. Such studies are needed for more precise quantification of the nonideal effects, particularly near and above the no-wall β limit and for the dynamics of mode-locking. The nonideal effects are also needed to obtain the proper Lagrangian perturbation $\delta \mathbf{B}^L$ and hence δB_n^L for NTV torque. Most recently, experimental studies of plasma response effects have moved on to explore the combined effects of 3D fields and toroidal plasma rotation in stabilizing RWMs above the no-wall β limit — see the next section.

7. Low n Plasma-Instability-Induced $\delta \mathbf{B}$ s And Their 3D Field Effects

Direct effects: Classical and neoclassical tearing modes (NTMs) and resistive wall modes (RWMs) cause additional 3D magnetic perturbations in tokamak plasmas. Direct effects of these MHD-type instabilities are: 1) RWM-induced $\delta B_n(\psi, m)$ perturbations cause non-resonant low n NTV effects via (8); and 2) Nonlinear tearing modes bifurcate the magnetic topology and form magnetic islands within the plasma that modify and complicate NTV effects [18]. Lagrangian contributions to δB_n must also be taken into account for RWMs and in non-resonant regions outside magnetic islands.

Resistive wall modes (RWMs) [90]: Above the no-wall β limit, low n (typically $n = 1, 2$) ideal MHD-type RWMs are stabilized if Ω_t is large enough [91, 92, 30, 31] for the resistive wall to represent a conducting wall to the rotating plasma. If the plasma is stationary, magnetic field perturbations penetrate the resistive wall and RWMs can become unstable. Very recent experiments have demonstrated that the minimum Ω_t is lower than previously thought [93, 94, 33], apparently because of stabilizing kinetic-based effects [95] due to thermal and fast ions [96, 97, 98, 99] whose toroidal precessional drift frequencies resonate with the plasma rotation frequency ω . Even when RWMs are stabilized they increase RFA of the $n = 1$ $\delta\mathbf{B}$ in the plasma, as indicated in figure 9. The resultant Lagrangian $\delta\mathbf{B}^L$ increases the NTV damping of Ω_t , the sensitivity to low n field errors and the tendency for NTMs to be excited.

Tearing modes [100]–[105], [63]: For relevant β values the bootstrap current provides a source of free energy for “neoclassical tearing modes” (NTMs, [102, 103, 104, 105]) in addition to the usual Δ' current gradient source [100]. Tearing modes can be nonlinearly excited into the nonlinear Rutherford regime [101] by low m/n (typically 3/2 and 2/1) magnetic perturbations or they can appear “spontaneously.” The critical issue for both classical (Δ' -driven, [100, 101]) and neoclassical (bootstrap-current-driven, [102]–[105]) tearing modes is: what is the nonlinear excitation threshold [104, 106] $\delta B_{\rho m/n}$ for given combinations of the normalized β_N and plasma toroidal rotation Ω_t . Recent experiments indicate that the threshold is more easily exceeded at lower β_N as Ω_t is reduced [107]–[110], perhaps because Δ' is influenced by flow shear as indicated by some recent simulation studies [111]. When tearing modes occur they modify [15, 18] the radial ion flux and NTV torque in the vicinity of the island; then NTV effects become more complicated and larger [18], with possible kinetic reductions due to reactive resonant Pfirsch-Schlüter current effects on the island width [112].

8. Multiple Resonant Magnetic Perturbations (RMPs for ELMs)

The pioneering use of resonant magnetic perturbations (RMPs) on DIII-D [113]–[119] to control edge localized modes (ELMs) is predicated on edge magnetic stochasticity [120]–[122] to reduce edge plasma gradients in H-mode plasmas. Magnetic field stochasticity is caused by island overlap, as embodied in the Chirikov criterion [123, 124]. Key RMP effects are explained by this criterion, especially the “resonance-type” sensitivity to q_{95} ($\sim 11/3$ [113]–[119]) and divertor flux patterns. However, some effects may not be: electron heat transport is only slightly changed in the steep gradient region of H-mode pedestals but some density “pump-out” often occurs and ELM coils in some experiments trigger [125] or only mitigate [126] ELMs. Many possible RMP effects are currently being explored: 1) Most importantly, “screening” of RMP fields by Ω_t reduces the width of or even prevents the formation of magnetic islands and hence of the possibly stochastic region [74], [127]–[133]. 2) Density pump-out due to RMP-induced $\mathbf{E} \times \mathbf{B}$ cells [127], large $\boldsymbol{\xi} \cdot \nabla \rho$ near the X-point [77, 128], q_{95} resonances [133] or turbulence [134]; 3) Collision lengths comparable to the magnetic decorrelation length in

the pedestal [118]. 4) Possible “laminar” helical ribbons of magnetic flux in the pedestal, SOL regions [135, 136, 137]. 5) Radial plasma current driven by the combination of E_ρ and magnetic stochasticity [138]. And 6) Simulations of kinetic effects of RMPs on the pedestal [139, 140]: flow screening of RMPs, reduced pedestal E_ρ for density pump-out, and particle-trapping reduction effects on magnetic-flutter-induced [141] Rechester-Rosenbluth [142] transport. The precise mechanisms by which RMPs affect the pedestal and hence ELMs are still being clarified. However, RMP effects are stimulating interesting studies and developing tools for modifying edge plasma transport (density, temperatures and Ω_t) and associated edge stability.

9. Effects Of 3D Fields On Plasma Toroidal Rotation And Transport

Rotation profile evolution: As the preceding discussion has indicated, 3D fields can directly affect plasma toroidal rotation [and hence from (7) the radial electric field] via resonant field errors (for $\delta B_{\rho m/n}/B_0 \gtrsim 10^{-4}$), NTV (for $\delta B_n/B_0 \gtrsim 10^{-3}$) and toroidal field ripple (for $\delta B_N/B_0 \gtrsim 10^{-2}$). Sufficiently large resonant fields in the plasma cause its toroidal rotation at the rational surface to lock to the wall [$\omega(\rho_{m/n}) \rightarrow 0$]; thereafter the rest of the $\Omega_t(\rho)$ profile relaxes slowly [143] via the diffusive radial transport fluxes in (4). Tearing-mode-induced magnetic islands have the same effect. In contrast, the NTV and ripple effects globally damp Ω_t toward an offset frequency $\Omega_* < 0$. These Ω_t evolution scenarios are illustrated in figure 12. As can be seen in figure 12a, the NTV induced by a non-resonant 3D field globally reduces the toroidal plasma rotation. In contrast, as shown in figure 12b, a resonant tearing mode first abruptly reduces the toroidal plasma rotation where the island is; thereafter, this localized change in Ω_t slowly spreads radially due to χ_{ζ_i} -induced Ω_t diffusion.

Other effects on plasma transport: Concomitant density and heat transport fluxes induced by 3D field effects are of order $\varrho_*^2 (B_t/B_p)^2$ smaller [3]–[5] and hence usually negligible. Thus, theory predicts that 3D fields directly affect Ω_t but only indirectly affect net ambipolar density and energy transport — mainly through effects [11, 12] of changes in $\Omega_t(\rho)$ on microturbulence-induced n and T transport. Experimental results generally confirm this prediction in that they typically find that 3D fields can significantly affect Ω_t via field error, NTV and ripple effects but usually have much smaller (factors of 3 or greater) effects on n and T profiles. However, as the preceding section noted, sufficiently large, multiple RMPs may induce local magnetic stochasticity or other effects in the edge plasma and thereby increase n_e and T_e transport there. Thus, in general one can think of 3D fields primarily as tools for modifying the plasma toroidal rotation with much smaller and/or possible locally resonant direct effects on density and energy transport.

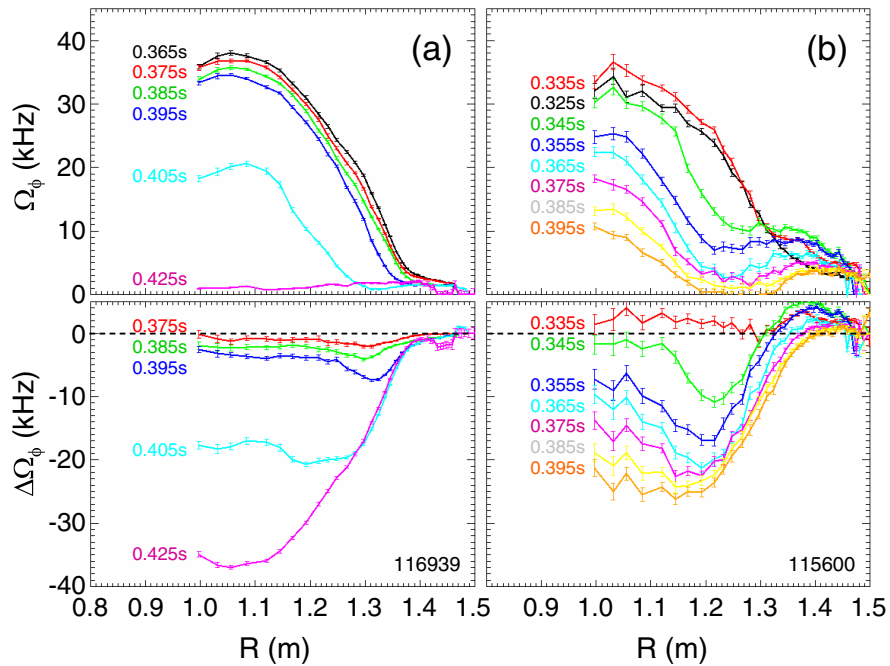


Figure 12. NSTX toroidal plasma rotation profiles versus major radius, and difference between initial and subsequent profiles for rotation damping [32]: a) during application of a 3D-field-induced NTV torque similar to that shown in figure 2 and (b) during excitation and locking of a rotating tearing instability.

10. Status, Open Issues (toward predictive capability for ITER)

Test blanket modules (TBMs): Recent experiments were performed [144, 145] on DIII-D to explore possible effects of field errors introduced by ITER test blanket modules (TBMs, $\delta \equiv \delta B/B_0 \sim 1.2\%$). The TBM mock-up was toroidally localized ($\Delta\zeta \sim 2\pi/24$) with $\delta \sim 1\text{--}3\%$. Its main effect was braking of Ω_t ($\propto \Omega_t$) with increasing δ , causing $\Delta\Omega_t/\Omega_t$ up to -50% (for $\beta_N \gtrsim 2$). Changes in density, confinement and β were factors of $\gtrsim 3$ smaller. Mode locking sensitivity to the $n=1$ field was greater, especially for higher β and lower Ω_t , but it was easily compensated. A major issue for the previously described theory is that since the TBM is toroidally localized, it is represented by a very large δB_n Fourier spectrum ($\pm n$ up to $\gg 2 \times 24$ coils). New NTV, FE and RFA theory needs to be developed for a delta-function toroidal field ripple. In the meantime, 3D effects in the TBM test have been estimated by summing over all the significant Fourier δB_n coefficients [146]. TBM test results were consistent with the modeling of these 3D effects [144, 146]. Global NTV Ω_t braking was semi-quantitatively predicted [144, 146] by IPEC [75] calculations. The very small TBM-induced $n=1$ edge field error is amplified by a large factor [146] ($\gtrsim 10$ for $\beta_N \gtrsim 2$) in the core by edge coupling to a stable, weakly damped $n=1$ kink. The I-coil compensation of the TBM-induced $n=1$ field error was also semi-quantitatively matched [144, 146] by IPEC calculations. Fast ion losses induced by the TBM were found [145] to be negligibly small

($\sim 1\text{--}5\%$). They could however cause significant local heating in the wall regions where the lost fast ion orbits intersect the vacuum chamber. Finally, the TBM mainly affected Ω_t , with lesser effects on n, T transport (albeit with a slight density pump-out).

Status Of 3D Effects: As discussed above, the fundamental physics building blocks of NTV, ripple, field error and RFA effects of low and medium n 3D fields on plasma toroidal rotation are approaching predictive capabilities for present experiments. Studies of “combined” effects of 3D fields on RWMs, NTMs and ELMs via RMPs are in a more developmental stage. Non-resonant 3D magnetic perturbations can be used to globally control toroidal plasma rotation. Resonant magnetic perturbations can modify Ω_t and possibly plasma transport in resonant regions of the plasma.

Possible implications for ITER: The $N = 18$ toroidal field system in ITER [1, 2] is projected to have relatively large ripple, even with FSTs ($\delta \lesssim 0.4\%$). Also, smaller toroidal torque densities will be induced in ITER by heating sources (e.g., NBI). Thus, the ripple-induced NTV toroidal torques will likely be dominant in (4). Hence, ITER plasmas will likely [37, 49] rotate toroidally with a frequency near the diamagnetic-level $\Omega_* < 0$ in (9), i.e., in the counter-current direction, at least over the outer region of the plasma. This lower, diamagnetic-level plasma toroidal rotation could produce some undesired effects: 1) greater sensitivity to $n = 1$ external 3D field errors and β that could induce locked modes?, 2) smaller radial electric field shear with less stabilization effects on microturbulence?, 3) reduced β_N thresholds for NTMs?, and 4) more reliance on kinetic ion effects to stabilize RWMs above the no-wall limit? Non-resonant fields in ITER may be able to use NTV effects to control $\Omega_t(\rho, t)$. Error field sensitivities in ITER have been estimated using the IPEC code [147]. Some additional important 3D field effects issues for ITER are: 1) the precise 3D RMP field characteristics required for stabilization or amelioration of ELMs, 2) density “pump-out” caused by FEs, RMPs and ripple, which is not yet understood, 3) RFA effects on $n=1$ fields in plasmas including two-fluid layer and low collisionality physics, and 4) determination of how small field errors must be to avoid locked modes as β is increased — and an assessment of the degree to which internal, dynamic field error compensation coils might be needed.

Acknowledgments

The author is grateful to many colleagues who provided perspectives on the key 3D field effects issues that should be addressed in this invited theory-based overview talk OV/4-3 at the 23rd International Atomic Energy Agency Fusion Energy Conference, 12-16 October 2010 in Daejeon, Korea. The author is particularly grateful to R.J. Buttery, A.M. Garofalo, M.J. Lanctot, H. Reimerdes, S.A. Sabbagh, O. Schmitz, M. Yoshida, A.J. Cole, C.C. Hegna and C.R. Sovinec for useful discussions of various key issues and for comments on early drafts of this manuscript. This research was supported by U.S. DoE grants DE-FG02-86ER53218 and DE-FG02-92ER54139.

References

References presented below with paper designators (e.g., EXS/P3-06) were presented at this 23rd International Atomic Energy Agency (IAEA) Fusion Energy Conference (FEC), 11-16 October 2010, Deajeon, Korea. They are available online at <http://www-naweb.iaea.org/napc/physics/FEC/FEC2010/html/index.htm>.

Glossary for references

ITER: [1, 2]

Transport equations: [3]–[8]

Stellarator transport background: [9], [10]

High n microturbulence effects on toroidal flow: [11], [12]

Neoclassical toroidal viscosity (NTV) theory: [13]–[25], [9], [10]

Neoclassical toroidal viscosity (NTV) experiments: [26]–[44], [67], [99]

Return current induced by direct ion losses: [45], [4]

Ripple experiments: [46]–[55]

Field errors: [56]–[70], [31], [35], [44]

Plasma responses: [71]–[89], [21], [31], [32], [37], [66]–[69]

Resistive wall modes (RWMs): [90]–[99], [30]–[33], [67]–[69], [88], [89]

Tearing modes: [100]–[112], [63]

Multiple resonant magnetic perturbation (RMP) effects: [113]–[142], [74], [77]

Effects of rotation on plasma: [143], [3]–[5], [30], [32]

Test blanket module (TBM) effects: [144], [145]

ITER field errors: [146], [147]

- [1] Aymar R., Chuyanov V.A., Huguet M., Shimomura Y. ITER Joint Central Team and ITER Home Teams 2001 *Nucl. Fusion* **41** 1301
- [2] Shimada M. *et al* 2007 *Nucl. Fusion* **47** S1
- [3] Callen J.D., Cole A.J. and Hegna C.C. 2009 *Nucl. Fusion* **49** 085021
- [4] Callen J.D., Cole A.J. and Hegna C.C. 2009 *Phys. Plasmas* **16** 082504
- [5] Callen J.D., Hegna C.C. and Cole A.J. 2010 *Phys. Plasmas* **17** 056113
- [6] Pustovitov V.D. 2011 *Nucl. Fusion* **51** 013006
- [7] Hinton F.L. and Hazeltine R.D. 1976 *Rev. Mod. Phys.* **48** 239
- [8] Hirshman S.P. and Sigmar D.J. 1981 *Nucl. Fusion* **21** 1079
- [9] Shaing K.C. and Callen J.D. 1983 *Phys. Fluids* **26** 3315
- [10] Shaing K.C., Callen J.D. and Hirshman S.P. 1986 *Phys. Fluids* **29** 521
- [11] Diamond P.H. *et al* 2009 *Nucl. Fusion* **49** 045002
- [12] Peeters A.G. *et al* “Toroidal Momentum Transport,” submitted to *Nucl. Fusion* (February 2011)
- [13] Shaing K.C. 2003 *Phys. Plasmas* **10** 1443
- [14] Shaing K.C. *et al* 2008 *Phys. Plasmas* **15** 082506
- [15] Shaing K.C., Sabbagh S.A. and Chu M.S. 2009 *Plasma Phys. Control. Fusion* **51** 035009
- [16] Shaing K.C., Sabbagh S.A. and Chu M.S. 2010 *Nucl. Fusion* **50** 025022
- [17] Shaing K.C. and Callen J.D. 1982 *Nucl. Fusion* **22** 1061
- [18] Shaing K.C. *et al* “Theory for Neoclassical Toroidal Plasma Viscosity in Tokamaks,” submitted to *Nucl. Fusion* (January 2011)
- [19] Goldston R.J., White R.B. and Boozer A.H. 1981 *Phys. Rev. Lett.* **47** 647
- [20] Park J-K., Boozer A.H. and Menard J.E. 2009 *Phys. Rev. Lett.* **102** 065002
- [21] Park J-K. *et al* 2009 *Phys. Plasmas* **16** 056115
- [22] Shaing K.C., Chu M.S. and Sabbagh S.A. 2009 *Plasma Phys. Control. Fusion* **51** 075015
- [23] Stix T.H. 1962 *The Theory of Plasma Waves* (New York: McGraw-Hill) p 206
- [24] Cole A.J., Hegna, C.C. and Callen J.D. “Low Collisionality Neoclassical Toroidal Viscosity in Tokamaks and Quasi-symmetric Stellarators Using an Integral-truncation Technique,” UW-

- CPTC 08-8, 26 June 2009, available via <http://www.cptc.wisc.edu>.
- [25] Cole A.J., Hegna, C.C. and Callen J.D. “Multi-collisionality neoclassical toroidal viscosity using Langer’s method,” UW-CPTC 11-6, June 2011, to be made available via <http://www.cptc.wisc.edu>.
- [26] La Haye R.J. *et al* 2002 *Phys. Plasmas* **9** 2051
- [27] Lazzaro E. *et al* 2002 *Phys. Plasmas* **9** 3906
- [28] Gerhardt S.P., Talmadge J.N., Canik J.M. and Anderson D.T. 2005 *Phys. Rev. Lett.* **94** 015002
- [29] Gerhardt S.P., Talmadge J.N., Canik J.M. and Anderson D.T. 2007 *Phys. Plasmas* **12** 056116
- [30] Sabbagh S.A. *et al* 2004 *Nucl. Fusion* **44** 560
- [31] Sabbagh S.A. *et al* 2006 *Nucl. Fusion* **46** 635
- [32] Zhu W., Sabbagh S.A. *et al* 2006 *Phys. Rev. Lett.* **96** 225002
- [33] Sabbagh S.A. *et al* 2010 *Nucl. Fusion* **50** 025020
- [34] Sun Y. *et al* “Non-resonant magnetic braking on JET and TEXTOR,” EXS/P3-06
- [35] Cole A.J., Hegna C.C. and Callen J.D. 2007 *Phys. Rev. Lett.* **99** 065001
- [36] Garofalo A.M. *et al* 2008 *Phys. Rev. Lett.* **101** 195005
- [37] Garofalo A.M. *et al* 2009 *Phys. Plasmas* **16** 056119
- [38] Solomon W.M. *et al* 2009 *Nucl. Fusion* **49** 085005
- [39] Hua M-D., Chapman I.T. *et al* 2010 *Plasma Phys. Control. Fusion* **52** 035009
- [40] Cole A.J. *et al* “Peak neoclassical toroidal viscous force in the DIII-D tokamak,” oral paper O4.115, 37th Plasma Physics EPS meeting, Dublin, Ireland, 21-25 June 2010, available via <http://ocs.ciemat.es/EPS2010PAP/pdf/O4.115.pdf>.
- [41] Cole A.J. *et al* 2011 *Phys. Rev. Lett.* **106** 225002
- [42] Cole A.J. *et al* 2011 *Phys. Plasmas* **18** 055711
- [43] Garofalo A.M. *et al* “Advances Toward QH-mode Viability for ELM-Free Operation in ITER,” submitted to *Nucl. Fusion* (January 2011)
- [44] Gerhardt S.P. *et al* 2010 *Plasma Phys. Control. Fusion* **52** 104003
- [45] Hinton F.L. and Rosenbluth M.N. 1999 *Phys. Lett. A* **259** 269
- [46] Scott S.D. *et al* 1985 *Nucl. Fusion* **25** 359
- [47] Yoshida M. *et al* 2006 *Plasma Phys. Control. Fusion* **48** 1673
- [48] Honda M. *et al* 2008 *Nucl. Fusion* **48** 085003
- [49] de Vries P.C. *et al* 2008 *Nucl. Fusion* **48** 035007
- [50] Saibene G. *et al* in *Fusion Energy 2008* (Proc. 22nd Int. Conf. Geneva, 2008) (Vienna: IAEA) CD-ROM file EX/2-1 and <http://www-naweb.iaea.org/napc/physics/FEC/FEC2008/html/index.htm>.
- [51] Fenzi C. *et al* “On Plasma Rotation with Toroidal Magnetic Field Ripple and No External Momentum Input,” submitted to *Nucl. Fusion* (January 2011)
- [52] Urano H. *et al* “Comparison of pedestal characteristics in JET & JT-60U similarity experiments under variable toroidal field ripple,” submitted to *Nucl. Fusion* (January 2011)
- [53] Saibene G. *et al* 2007 *Nucl. Fusion* **47** 969
- [54] Yoshida M. *et al* “Core and edge toroidal rotation study in JT-60U,” submitted to *Nucl. Fusion* (January 2011)
- [55] Salmi A. *et al* 2008 *Contrib. Plasma Phys.* **48** 77
- [56] Nave M.F.F. and Wesson J.A. 1990 *Nucl. Fusion* **30** 2575
- [57] Hender T.C. *et al* 1992 *Nucl. Fusion* **32** 2091
- [58] Fitzpatrick R. 1993 *Nucl. Fusion* **33** 1049
- [59] Taylor J.B. 2003 *Phys. Rev. Lett.* **91** 115002
- [60] Fitzpatrick R. 1995 lecture on “Driven Reconnection in Magnetic Fusion Experiments,” available from <http://farside.ph.utexas.edu/papers/lecture.html>
- [61] Reiman A.H. and Monticello D. 1991 *Phys. Fluids B* **3**, 2230
- [62] Cole A. and Fitzpatrick R. 2006 *Phys. Plasmas* **13** 032503
- [63] F.L. Waelbroeck 2009 *Nucl. Fusion* **49** 104025

- [64] Cole A.J., Hegna C.C. and Callen J.D. 2008 *Phys. Plasmas* **15** 056102
- [65] Wolfe S.M. *et al* 2005 *Phys. Plasmas* **12** 056110
- [66] Park J.-K., Schaffer M.J., Menard J.E. and Boozer A.H. 2007 *Phys. Rev. Lett.* **99** 195003
- [67] Reimerdes H. *et al* 2009 *Nucl. Fusion* **49** 115001
- [68] Lanctot M.J. *et al* 2010 *Phys. Plasmas* **17** 030701
- [69] Menard J.E. *et al* 2010 *Nucl. Fusion* **50** 045008
- [70] Volpe F. University of Wisconsin, Madison, WI USA (2010 private communication)
- [71] Boozer A.H. 2001 *Phys. Rev. Lett.* **86** 5059
- [72] Boozer A.H. and Nührenberg C. 2006 *Phys. Plasmas* **13** 102501
- [73] Liu Y.Q. *et al* 2000 *Phys. Plasmas* **7** 3681
- [74] Chu M.S. *et al* "Response of a Resistive and Rotating Tokamak to External Magnetic Perturbations Below the Alfvénic Frequency," submitted to *Nucl. Fusion* (February 2011)
- [75] Park J.-K., Boozer A.H. and Glasser A.H. 2007 *Phys. Plasmas* **14** 052110
- [76] Glasser A.H. and Chance M.S. 1997 *Bull. Am. Phys. Soc.* **42** 1848
- [77] Liu Y.Q. *et al* "Modelling of Plasma Response to RMP Fields in MAST and ITER," submitted to *Nucl. Fusion* (February 2011)
- [78] Pustovitov V.D. 2007 *Nucl. Fusion* **47** 1583
- [79] Zheng L.-J., Kotschenreuther M. and Waelbroeck F.L. 2006 *Nucl. Fusion* **46** L9
- [80] Pustovitov V.D. 2009 *Nucl. Fusion* **49** 045003
- [81] W. Park *et al* 1999 *Phys. Plasmas* **6** 1696 (<http://w3.pppl.gov/m3d/index.php>)
- [82] Sovinec C.R. *et al* 2004 *J. Comp. Phys.* **195**, 355 (<https://nimrodteam.org>)
- [83] Huysmans G.T.A., Hender T.C., Hawkes N.C. and Litaudon X. 2001 *Phys. Rev. Lett.* **87** 245002
- [84] Callen J.D. and Shaing K.C. 1985 *Phys. Fluids* **28** 1845
- [85] Wilson H.R., Connor J.W., Hastie R.J. and Hegna C.C. 1995 *Phys. Plasmas* **3** 248
- [86] La Haye R.J., Hyatt A.W. and Scoville J.T. 1992 *Nucl. Fusion* **32** 2119
- [87] Garofalo A.M. *et al* 1999 *Phys. Rev. Lett.* **82** 3811
- [88] Garofalo A.M. *et al* 2002 *Phys. Plasmas* **9** 1997
- [89] Reimerdes H. *et al* 2004 *Phys. Rev. Lett.* **93** 135002
- [90] Freidberg J.P. 1987 *Ideal Magnetohydrodynamics* (New York: Plenum, New York)
- [91] Strait E.J. *et al* 1995 *Phys. Rev. Lett.* **74** 2483
- [92] Garofalo A.M. *et al* 2002 *Phys. Rev. Lett.* **89** 235001
- [93] Reimerdes H. *et al* 2007 *Phys. Rev. Lett.* **98** 055001
- [94] Strait E.J. *et al* 2007 *Phys. Plasmas* **14** 056101
- [95] Hu B., Betti R. 2004 *Phys. Rev. Lett.* **93** 105002
- [96] Berkery J.W. *et al* 2010 *Phys. Plasmas* **17** 082504
- [97] Reimerdes H. *et al* "Non-ideal Modifications of 3D Equilibrium and Resistive Wall Mode Stability Models in DIII-D," EXS/5-4
- [98] Reimerdes H. *et al* *Phys. Rev. Lett.* **106** 215002
- [99] Sabbagh S.A. *et al* "Resistive Wall Mode Stabilization and Plasma Rotation Damping Considerations for Maintaining High Beta Plasma Discharges in NSTX," EXS/5-5
- [100] Furth H.P., Killeen J., Rosenbluth M.N. 1963 *Phys. Fluids* **6** 459
- [101] Rutherford, P.H. 1973 *Phys. Fluids* **16** 1903
- [102] Callen J.D. *et al* in *Plasma Physics and Controlled Nuclear Fusion Research 1986* (IAEA, Vienna, 1987), Vol. 2, p 157
- [103] Carrera, R., Hazeltine, R.D. and Kotschenreuther M. *Phys. Fluids* **29**, 899 (1986).
- [104] Chang Z., Callen J.D., Fredrickson E.D. *et al* 1995 *Phys. Rev. Lett.* **74** 4663
- [105] La Haye R.J. 2006 *Phys. Plasmas* **13** 055501
- [106] Mikhailovskii A.B. 2003 *Contrib. Plasma Phys.* **43** 125
- [107] Buttery R.J. *et al* 2008 *Phys. Plasmas* **15** 056115
- [108] La Haye R.J. and Buttery R.J. 2009 *Phys. Plasmas* **16** 022107
- [109] La Haye R.J., Brennan D.P., Buttery R.J., and Gerhardt S.P. 2010 *Phys. Plasmas* **17**, 056110

- [110] Buttery R.J. *et al* 2011 *Nucl. Fusion* **51** 073016
- [111] Maget P. *et al* "Effect of rotation on the modelled NTM threshold in JET Advanced Scenarios," oral paper O2.104, 37th Plasma Physics EPS meeting, Dublin, Ireland, 21-25 June 2010, available via <http://ocs.ciemat.es/EPS2010PAP/pdf/O2.104.pdf>.
- [112] Hegna C.C. *et al* "High-beta physics of magnetic islands in 3-D equilibria," THS/4-1
- [113] Evans T.E. *et al* 2004 *Phys. Rev. Lett.* **95** 235003
- [114] Evans T.E. *et al* 2005 *Nucl. Fusion* **45** 595
- [115] Evans T.E. *et al* 2006 *Nature Physics* **2** 419
- [116] Evans T.E. *et al* 2006 *Phys. Plasmas* **13** 056121
- [117] Evans T.E. *et al* 2008 *Nucl. Fusion* **48** 024002
- [118] Fenstermacher M.E. *et al* 2008 *Phys. Plasmas* **15** 056122
- [119] Fenstermacher M.E. *et al* "ELM Control by Resonant Magnetic Perturbations: Overview of Research by the ITPA Pedestal and Edge Physics Group," ITR/P1-30
- [120] Evans T.E. *et al* 1987 *J. Nucl. Mat.* **145-147** 812
- [121] Grosman A. 1999 *Plasma Phys. Control. Fusion* **41** A185
- [122] Ghendrih Ph. *et al* 2002 *Nucl. Fusion* **42** 1221
- [123] Chirikov B.V. 1979 *Sov. J. Plasma Physics* **4** 289
- [124] Chirikov B.V. 1979 *Physics Reports* **52** 263
- [125] Canik J.M. *et al* 2010 *Phys. Rev. Lett.* **104** 045001
- [126] Liang Y. *et al* 2007 *Phys. Rev. Lett.* **98** 265004
- [127] Izzo V.A. and Joseph I. 2008 *Nucl. Fusion* **48** 115004
- [128] Kirk A. *et al* "Magnetic perturbation experiments on MAST using internal coils," EXD/8-2
- [129] Strauss H.R. *et al* 2009 *Nucl. Fusion* **49** 055025
- [130] Bécoulet M. *et al* "Role of diamagnetic and neoclassical effects in non-linear MHD rotating plasma response to resonant magnetic perturbations," poster P4.104, 37th Plasma Physics EPS meeting, Dublin, Ireland, 21-25 June 2010, available via <http://ocs.ciemat.es/EPS2010PAP/pdf/P4.105.pdf>.
- [131] Sugiyama L. *et al* "Magnetic X-points, edge instabilities, and the H-mode edge," THS/P3-04
- [132] Yu Q. *et al* "Plasma Response to Externally Applied Resonant Magnetic Perturbations," submitted to *Nucl. Fusion* (January 2011)
- [133] Liang Y. *et al* 2011 *Nucl. Fusion* **51** 073001
- [134] Yan Z. *et al* "Pedestal Turbulence Dynamics in ELMing and ELM-Free H-Mode Plasmas," EXC/P3-05
- [135] Schmitz O. *et al* 2008 *Nucl. Fusion* **48** 024009
- [136] Schmitz O. *et al* 2009 *Phys. Rev. Lett.* **103** 165005
- [137] Schmitz O. *et al* "Key Results from the DIII-D/TEXTOR Collaboration on the Physics of Stochastic Boundaries projected to ELM Control at ITER," EXD/P3-30
- [138] Rozhansky V. *et al* "Modeling of the Edge Plasma of MAST in the Presence of Resonant Magnetic Perturbations," submitted to *Nucl. Fusion* (January 2011)
- [139] Park G. *et al* 2010 *Phys. Plasmas* **17** 102503
- [140] Chang C.S. *et al* "Self-consistent simulation of kinetic pedestal transport under RMP penetration," THC/P4-04
- [141] Callen, J.D. 1977 *Phys. Rev. Lett.* **39** 1540
- [142] Rechester A.B. and Rosenbluth, M.N. 1978 *Phys. Rev. Lett.* **40** 38
- [143] Yokoyama M., Callen J.D., and Hegna C.C. 1996 *Nucl. Fusion* **36** 1307
- [144] Schaffer M.J. *et al* "ITER Test Blanket Module Error Field Simulation Experiments at DIII-D," submitted to *Nucl. Fusion* (February 2011)
- [145] Kramer G.J. *et al* "Fast Ion Effects during Test Blanket Module Simulation Experiments in DIII-D," EXW/P7-10
- [146] Park J-K. *et al* "Robust correction of 3D error fields in tokamaks including ITER," EXS/P5-12
- [147] Park J-K., Boozer A.H., Menard J.E. and Schaffer M.J. 2008 *Nucl. Fusion* **48** 045006